

Growth and Characterization of Polycrystalline NbO₂ Thin Films on Crystalline and Amorphous Substrates

Ali Fakih,¹ Johan Biscaras,^{1,*} and Abhay Shukla^{1,†}

¹*Institut de Minéralogie, de Physique des Matériaux et de Cosmochimie,
Sorbonne Université, UMR CNRS 7590,
MNHN, 4 Place Jussieu, F-75005 Paris, France*

Abstract

NbO₂ is a potential material for nanometric memristor devices, both in the amorphous and the crystalline form. We fabricated NbO₂ thin films using RF-magnetron sputtering from a stoichiometric target. The as-deposited films were amorphous regardless of the sputtering parameters. Post deposition vacuum annealing of the films was necessary to achieve crystallinity. A high degree of crystallinity was obtained by optimizing annealing duration and temperature. The resistivity of the material increases as it undergoes a structural transition from amorphous to crystalline with the crystalline films being one order of magnitude more resistive.

DOI:

PACS numbers:

INTRODUCTION

Niobium dioxide NbO_2 exhibits an insulator-metal transition at about 800 °C which transforms the low temperature insulating phase with a room temperature resistivity ρ of $2 \times 10^2 \Omega\cdot\text{m}$ [1] into a metal with a resistivity of $1.4 \times 10^{-3} \Omega\cdot\text{cm}$ [2]. This phase transition is accompanied by a structural transition from a distorted rutile phase space group ($I4_1/a$) to a rutile phase space group ($P4_2/mnm$) [3–6]. Whether this phase transition is of the kind found in its parent metal oxide VO_2 at a much lower temperature is an open question, but the high temperature associated with it, and thus the stability of the low temperature phase has motivated several groups to study NbO_2 based devices [7–12]. These devices also show a sizeable change in resistance on the application of current, or more accurately, a current controlled negative differential resistance regime [12]. While devices often use variable stoichiometry NbO_x (with x varying from 2 to 2.5) and amorphous as-deposited phases which eventually crystallize with temperature or voltage [10], it is desirable to directly grow the NbO_2 phase, both amorphous and crystalline, on a variety of substrates, using a single, reproducible method. Numerous works have reported the growth of NbO_2 films using evaporation [13–16], deposition [1, 17, 18] or sputtering techniques [19–26] with either in-situ or post-deposition oxidation and crystallization on various substrates ranging from glass to single crystal silicon.

The targets used have been variously Nb or stoichiometric NbO_2 with oxygen or argon partial pressure during deposition. Post deposition annealing, eventually in an oxidizing atmosphere has also been used. For example, NbO_2 thin films with nanoslice structures were obtained on silicon substrate by using reactive magnetron sputtering on a niobium target in Ar/O_2 atmosphere [19]. Epitaxial NbO_2 thin films were fabricated on Al_2O_3 substrates using reactive bias target ion beam deposition [17]. Recently Nakao et al.[1] demonstrated that NbO_2 films can be grown with pulsed laser deposition in a partial pressure of oxygen using a stoichiometric target. To attain crystallinity their samples were annealed after deposition in vacuum at a temperature of 600°C. However, it was also noted that the resistivity obtained for their samples remained significantly below the resistivity of bulk NbO_2 . Amorphous NbO_2 has a lower resistivity than crystalline NbO_2 , and thus low resistivity in thin films samples implies imperfect crystallization or eventually a deficient oxygen stoichiometry. For

reference, bulk resistivity of NbO_2 is $1 \times 10^4 \Omega \cdot \text{cm}$ [1] and that of Nb_2O_5 is $2 \times 10^7 \Omega \cdot \text{cm}$ [27]. In between these two phases NbO_2 (Nb charge state 4+) and Nb_2O_5 (Nb charge 5+) several non-stoichiometric, polymorphic or meta-stable phases exist which complicates fabrication of pure phases, especially that of NbO_2 [1, 13–26, 28].

MATERIALS AND METHODS

To directly deposit stoichiometric NbO_2 on the substrate, we chose RF magnetron sputtering avoiding partial oxygen pressure during deposition. We decided to concentrate on adequate conditions for deposition such as sputtering rate, substrate temperature and Ar partial pressure to obtain thin films with the good stoichiometry, followed by vacuum annealing for crystallization.

Parameter	Target Etching	Substrate Etching	Deposition
Ar pressure (mbar)	0.5	0.5	0.5
power (Watts)	100	225	225
voltage (V)	465	480	500
target-substrate distance (cm)	6.5	6.5	6.5
substrate temperature ($^{\circ}\text{C}$)	RT	RT	550
time (min)	2	3	4

TABLE I. Optimized sputtering parameters for stoichiometric NbO_2 thin films.

The stoichiometric target was obtained from Edgetech Industries LLC. It is important to verify that the target presents a uniform dark blue-grey colour characteristic of the NbO_2 phase. A light coloured target is a sign of oxidation during the sintering phase of the target even if the powder precursor is stoichiometric NbO_2 . The NbO_2 phase of the chosen target was verified by Raman spectroscopy and X-Ray diffraction (XRD) before mounting in the sputtering chamber. Nominal stoichiometry for the target does not imply phase purity and stoichiometry of the deposited film and may be the reason why oxygen or argon, and in some cases hydrogen [29] partial pressure has been necessary in earlier experiments. However oxidation or reduction during film deposition is a delicate adjustment which can

also influence deposition dynamics.

An important aspect of our methodology was to ensure a similar fabrication process for films on three different substrates, soda-lime glass, single crystal silicon and single crystal silicon topped by a 285 nm layer of poly-crystalline oxide. Of these, the glass substrate constrains annealing to temperatures below 600° C, while the other substrates may be annealed at higher temperatures. The parameters varied to optimize the quality of the deposited films were total magnetron power, the process gas (Ar) pressure, sample target distance which control the sputtering rate and finally substrate temperature which can alter deposition dynamics and notably help crystallization. Several depositions were made with the three kinds of substrates by varying these parameters. We observed that the dominant parameter controlling the film quality was the Ar pressure. The final optimal parameters for each of the substrates are collected in table I.

The Raman Spectroscopy measurements were performed using an Xplora Raman spectrometer (HORIBA Jobin-Yvon) with a monochromatic laser of 532 nm wave length, and the XRD instrument used was Panalytical Xpert Pro MPD diffractometer with a cobalt cathode ray tube as an x-ray source having $\lambda_{Co} = 1.790 \text{ \AA}$. XRD experiments were measured in two different configurations: (1) Bragg Brentano (BB) and (2) grazing incidence (GI) with an angle fixed at 1°. In thin films (some samples were only 30 nm thick) the grazing incidence mode helps to maximize the signal from the sample and minimize the signal from the substrate. Both Raman scattering and XRD were used to check the phase of the poly-crystalline films. Finally, we optimized post-annealing temperature for each substrate and characterized sample quality using optical micrographs, XRD, Raman scattering and transport measurements.

RESULTS AND DISCUSSION

Using the parameters presented in table I, amorphous films were obtained on all three substrates regardless of the substrate temperature as verified by both Raman spectroscopy and XRD. Trace crystalline structure was obtained on the Si and SiO₂/Si. The deposition rate was about 33 nm/min as measured by AFM. After the deposition, an annealing

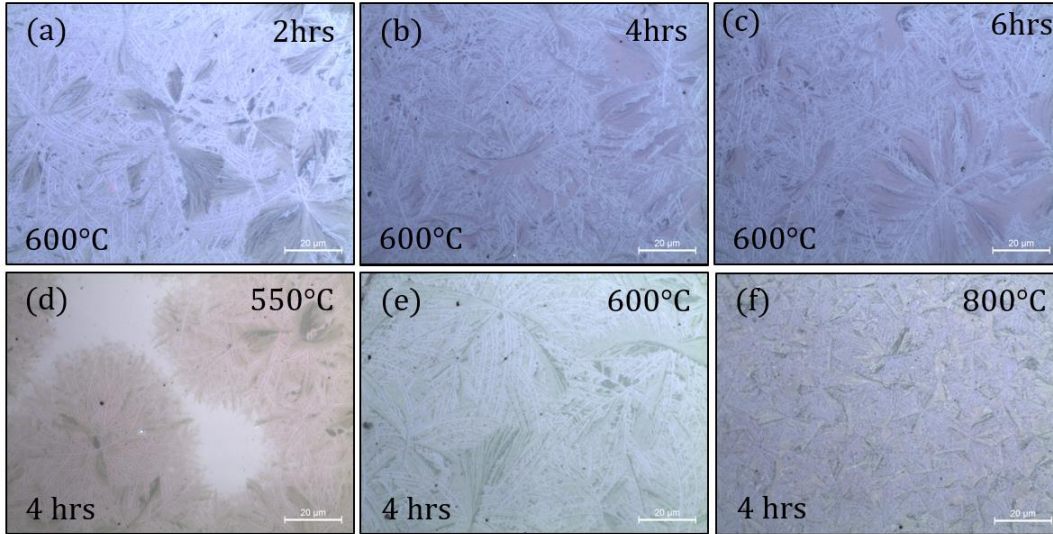


FIG. 1. Optical images of 330 nm NbO_2 films. Films on glass substrates annealed at different times (a) 2hrs (b) 4hrs (c) 6hrs. Films on Si substrates annealed at different temperatures (d) 550 °, non crystalline regions remain in the film (e) 600°C (f) 800°C.

procedure was then implemented to induce crystallization in the samples. Keeping in mind possible oxidation to the unwanted Nb_2O_5 phase in an oxidizing environment, we used vacuum annealing of the as-deposited films which yielded large area poly-crystalline films.

A typical branching microstructure (see Figure 1) appears on crystallization and is identified as NbO_2 with micro Raman spectroscopy. Optical inspection shows that microstructure size and density changes with annealing time (Figure 1 (a), (b) and (c), for NbO_2 films on glass). The annealing temperature plays a crucial role in crystallization since below about 525°C crystallization does not occur. On increasing the annealing temperature (Figure 1 (d), (e) and (f), NbO_2 film on Si) we notice that crystallization is not complete at 550°C (Figures 1 (d)), while above 600°C (Figures 1 (e) and (f)) microstructure size and density appear homogeneous.

Raman spectra of the NbO_2 films deposited on different substrates (glass, Si, and SiO_2) are shown in Figure 2. These spectra match those of nanostructured NbO_2 thin films pre-

pared by different methods [13, 17, 30].

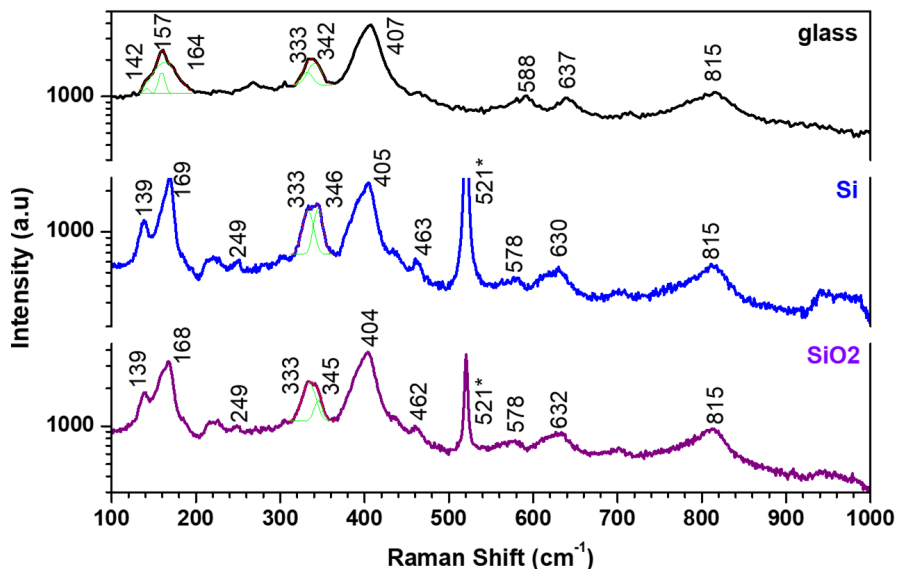


FIG. 2. The Raman Spectra of NbO₂ films deposited on different substrates: glass, Si < 100 > , and SiO₂. The 521 cm⁻¹ peaks come from the silicon substrate.

XRD measurements are shown in the standard Bragg Brentano (BB) geometry (Figures 3 (a) and (b)) and the Grazing Incidence (GI) geometry (Figures 3 (c) and (d)). In the as-deposited samples on the three substrates (Figures 3 (a) and (b)) only the films on the SiO₂/Si substrate show signs of crystallized phases of both NbO₂ and Nb₂O₅ [31–39]. Trace NbO₂ or Nb₂O₅ peaks on all three substrates are visible in the grazing incidence spectra. After vacuum annealing, all the three samples show the crystallized NbO₂ phase. Trace contributions from crystallized Nb₂O₅ are visible in the GI spectra. It is well-known [24] that exposure of NbO₂ thin films to air can lead to a surface Nb₂O₅ layer. Nevertheless, the quality of the films can be attested by the dominant NbO₂ peaks.

The grain size of the NbO₂ crystallites composing the films was estimated to be between 20 and 40 nm from the peak widths of diffractograms measured in BB geometry using the Scherrer equation:

$$\tau = \frac{K \lambda}{\beta \cos \theta}$$

where τ is the mean size of the crystallites which may be smaller or equal to the grain size, K is a dimensionless shape factor with a typical value of 0.9, λ is the x-ray wave length,

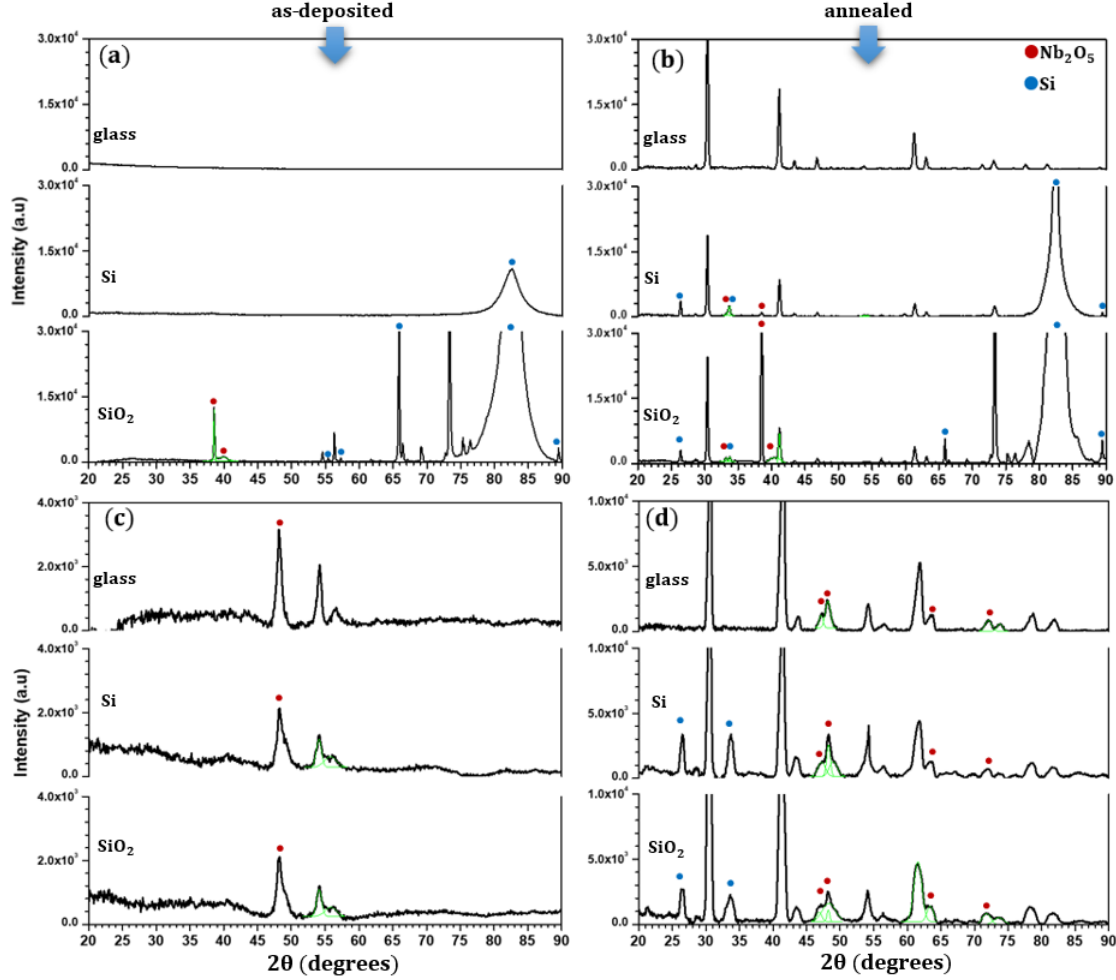


FIG. 3. X-ray diffractograms of NbO₂ films on different substrates: glass, Si and SiO₂ before and after annealing them. Figures (a) and (b) show the results of experiments done in the Bragg-Brentano configuration, while figures (c) and (d) show the results of experiments done in the grazing incidence geometry.

β is the peak broadening at half the maximum intensity (FWHM) and θ is the Bragg angle.

Raman Spectroscopy was also used to identify the crystalline phases in the sample. While the amorphous as-deposited films were featureless, annealed films showed peaks corresponding to the NbO₂ phase only. No other features corresponding to Nb₂O₅ or other parasite phases were found on any of the films except for silicon peaks coming from the substrate. Raman spectra were used to quantify effects of annealing time and temperature. Figure 4 (a) shows the Raman spectra on a sample with a glass substrate after 2 and 4 hrs of anneal-

ing indicating that the NbO₂ signal to background ration is strengthened with increasing annealing time. The effect of annealing temperature is displayed in Figure 4 (b) where the strengthening of the NbO₂ signal to background ratio is even more remarkable, especially for the higher annealing temperature. These observations confirm the qualitative optical observations of Figure 1.

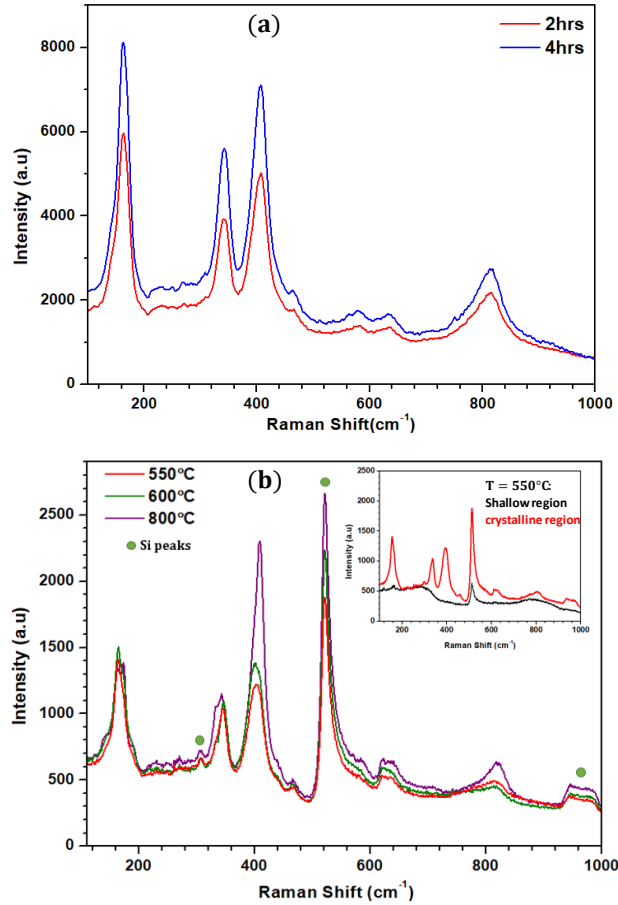


FIG. 4. Raman spectra showing the effect of annealing (a) time (NbO₂ film on glass substrate) and (b) temperature on the film quality (NbO₂ film on Si substrate) . Inset: The Raman spectrum of the shallow non-crystalline region of the sample whose structure is shown in figure 1 (d).

TRANSPORT PROPERTIES

Sheet resistance measurements were made on both amorphous and crystalline NbO₂ thin films on glass substrates. The room temperature resistivity of NbO₂ in existing literature

lacks consistency. Values reported for crystalline NbO₂ resistivity are for example, 200 Ω.cm [1], 2.5 Ω.cm [17], ~ 0.27 Ω.cm [40]. It is well-known that amorphous NbO₂ is less resistive and a better thermal conductor than crystalline NbO₂. Nakao et al. [1] find that their amorphous films have a resistivity as low as 0.27 Ω.cm, three orders of magnitude less than their crystalline films. Our crystalline films have a resistivity $\rho_{\text{cry}} \sim 54 \text{ } \Omega\cdot\text{cm}$ similar to that measured by Nakao et al. [1], but our amorphous films are only one order of magnitude less resistive ($\rho_{\text{amo}} \sim 4.5 \text{ } \Omega\cdot\text{cm}$). The scatter in the results cited for resistivity in literature probably arises from two sources. Firstly, partial crystallization will influence the measured value if the films are partially crystallized. To illustrate this we measured the resistance R_S of three 33 nm thick samples deposited on glass which were first vacuum annealed at 600°C for 2 hrs ($R=0.1 \text{ G}\Omega/\square$), 4 hrs ($R=0.2 \text{ G}\Omega/\square$) and 6 hrs ($R=0.3 \text{ G}\Omega/\square$). The increase in resistance with annealing time is in agreement with the earlier observations that the crystalline NbO₂ phase is more resistant than the amorphous one. Secondly, the stoichiometry is also very important since any deviation from the NbO₂ stoichiometry will change resistivity, with a decrease in resistivity if the film is oxygen deficient (NbO is metallic) and an increase in resistivity if the film is too rich in oxygen (Nb₂O₅ being a strong insulator).

Finally, we measured the temperature dependent resistivity of an amorphous film and a crystalline film deposited on glass substrates between 300 K and 400 K as shown in Figure 5 (a). The amorphous film is less resistive and as seen by the exponential decrease in resistivity with temperature, both display insulating behaviour each with a different activation energy. These activation energies are estimated from the linear fits in the Arrhenius plot of Figure 5 (b) to be ~ 0.27 eV and 0.18 eV for the crystalline and amorphous samples respectively.

CONCLUSIONS

We fabricated amorphous NbO₂ thin films (thickness between 33 and 330 nm) from a poly-crystalline target using RF-magnetron sputtering on three different substrates: glass, Si, SiO₂. The films were crystallized by annealing in vacuum at 600°C for films with glass substrates, and 600°C and above for Si based films. We observed that a longer annealing time and higher temperature lead to better polycrystalline film quality. The room temperature resistivities of the crystalline and amorphous samples were extracted from the

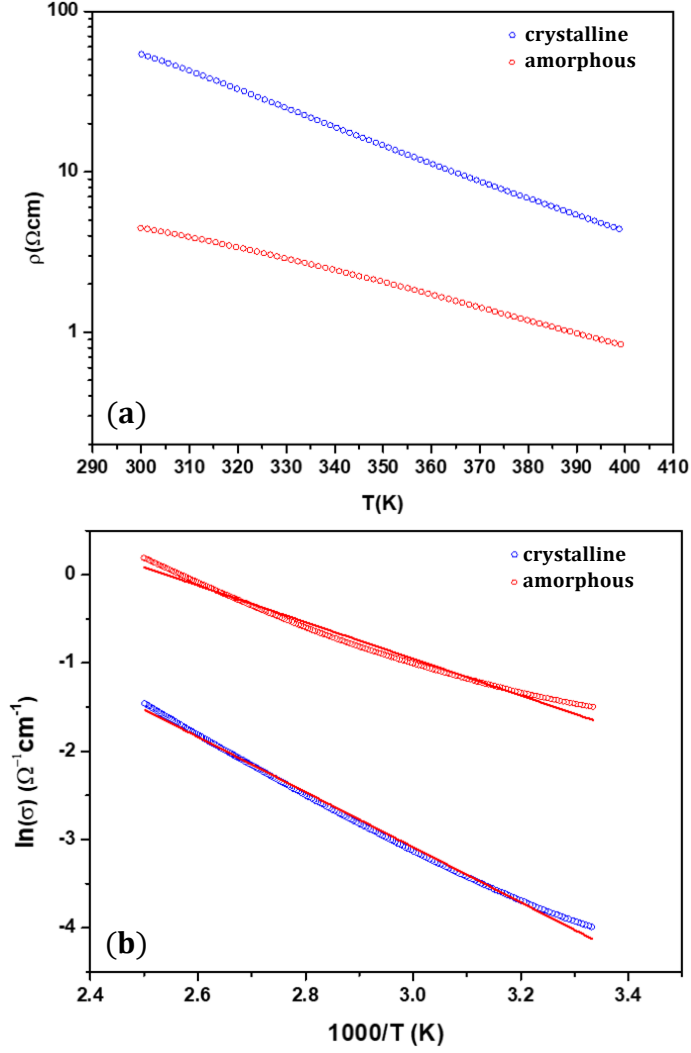


FIG. 5. (a) The resistivity of crystalline and amorphous NbO_2 films between 300 K and 400 K deposited on glass substrates. (b) The corresponding Arrhenius plots of the two samples from which the activation energy was extracted and found to be ~ 0.27 eV and 0.18 eV for the crystalline and amorphous samples respectively.

R_S measurements and were $\sim 54 \Omega\text{.cm}$ and $\sim 4.5 \Omega\text{.cm}$ respectively.

We acknowledge Benoit Baptiste and Ludovic Delbes for help with X-ray diffraction and Loic Becerra and Jean-Jacques Ganem for access to the clean room and vacuum furnace of the INSP. This work was supported by French state funds managed by the ANR within the Investissements d'Avenir programme under reference ANR-11-IDEX-0004-02, and more

specifically within the framework of the Cluster of Excellence MATISSE led by Sorbonne Universités.

* johan.biscaras@sorbonne-universite.fr

† abhay.shukla@sorbonne-universite.fr

- [1] S. Nakao, H. Kamisaka, Y. Hirose, T. Hasegawa, Structural, electrical, and optical properties of polycrystalline NbO₂ thin films grown on glass substrates by solid phase crystallization, *Phys. Status Solidi A* 214, (2017) 1600604.
- [2] T. Sakata , K. Sakata, G. Höfer, T. Horiuchi, Preparation of NbO₂ single crystals by chemical transport reaction, *Journal of Crystal Growth* 12 (1972) 89.
- [3] R. F. Janninck, D. H. Whitmore, Electrical conductivity and thermoelectric power of niobium dioxide, *J. Phys. Chem. Solids* 27, (1966) 1183.
- [4] A. Bolzan, C. Fong, B. J. Kennedy, C. J. Howard, A powder neutron diffraction study of semiconducting and metallic niobium dioxide, *J. Solid State Chem.* 9 (1994) 113.
- [5] A. K. Cheetham, C. N. R. Rao, A neutron diffraction study of niobium dioxide, *Acta Crystallogr. B* 32, (1976) 1579.
- [6] R. Pynn, J. D. Axe, R. Thomas, Structural distortions in the low-temperature phase of NbO₂, *Phys. Rev. B* 13, (1976) 2965.
- [7] K. Jung, Y. Kim, Y. S Park, W. Jung, J. Choi, B. Park, H. Kim, W. Kim, J. Hong, H. Im, Unipolar resistive switching in insulating niobium oxide film and probing electroforming induced metallic components, *J. of Appl. Phys.* 109, (2011) 054511.
- [8] T. Joshi, T. R Senty, P. Borisov, A. D Bristow, D. Lederman, Preparation, characterization, and electrical properties of epitaxial NbO₂ thin film lateral devices, *J. Phys. D: Appl. Phys.* 48 (2015) 335308.
- [9] S. Slesazek, H. Mahne, H. Wylezich, A. Wachowiak, J. Radhakrishnan, A. Ascoli, R. Tetzlaff, T. Mikolajick, Physical model of threshold switching in NbO₂ based memristors, *RSC Adv.* 5, (2015) 102318.
- [10] Gary A. Gibson, S. Musunuru¹, J. Zhang¹, K.Vandenberghe, J. Lee¹, C. Hsieh, W. Jackson, Y. Jeon, D.Henze, Z. Li, R. Stanley Williams, An accurate locally active memristor model for S-type negative differential resistance in NbO_x, *Appl. Phys. Lett.* 108, (2016) 023505.

- [11] S. Kumar, J. Paul Strachan, R. Stanley Williams, Chaotic dynamics in nanoscale NbO₂ Mott memristors for analogue computing, *Nature* 548 (2017) 318.
- [12] S. Kumar, Z. Wang, N. Davila, N. Kumari, Kate J. Norris, X. Huang, J. Paul Strachan, D. Vine, A.L. David Kilcoyne, Y. Nishi, R. Stanley Williams, Physical origins of current and temperature controlled negative differential resistances in NbO₂, *Nat. commun.* 8 (2017) 658.
- [13] Y. Zhao, Z. Zhang, Y. Lin, Optical and dielectric properties of a nanostructured NbO₂ thin film prepared by thermal oxidation, *J. Phys. D* 37, (2004) 3392.
- [14] A. O'Hara, T. N. Nunley, A. B. Posadas, S. Zollner, A. A. Demkov, Electronic and optical properties of NbO₂, *J. Appl. Phys.* 116, (2014) 213705.
- [15] F. J. Wong, N. Hong, S. Ramanathan, Orbital splitting and optical conductivity of the insulating state of NbO₂, *Phys. Rev. B* 90, (2014) 115135.
- [16] A.B. Posadas, A. O'Hara, S. Rangan, R. A. Bartynski, A. A. Demkov, Band gap of epitaxial in-plane-dimerized single-phase NbO₂ films, *Appl. Phys. Lett.* 104, (2014) 092901.
- [17] Y. Wang, R. B. Comes, S. Kittiwatanakul, S. A. Wolf, J. Lu, Epitaxial niobium dioxide thin films by reactive-biased target ion beam deposition, *J. Vac. Sci. Technol. A* 33, (2015) 021516.
- [18] A. Bonakdarpour, R. T. Tucker, M. D. Fleischauer, N. A. Beckers, M. J. Brett, D. P. Wilkinson, Nanopillar niobium oxides as support structures for oxygen reduction electrocatalysts, *Electrochim. Acta* 85, (2012) 492.
- [19] D. Music, R. W Geyer, Theoretical and experimental study of NbO₂ nanoslice formation, *J. Phys. D: Appl. Phys.* 48 (2015) 305302.
- [20] C. Nico, T. Monteiro, M. P. F. GraSca, Niobium oxides and niobates physical properties: Review and prospects, *Prog. Mater. Sci.* 80, (2016) 1-37.
- [21] F. J. Wong, S. Ramanathan, Heteroepitaxy of distorted rutile-structure WO₂ and NbO₂ thin films, *J. Mater. Res.* 28, (2013) 2555.
- [22] A. Foroughi-Abari, K. C. Cadien, Growth, structure and properties of sputtered niobium oxide thinfilms, *Thin Solid Films* 519, (2011) 3068.
- [23] M. D. Pickett, G. Medeiros-Ribeiro, R. S. Williams, A scalable neuristor built with Mott memristors, *Nature Mater.* 12, (2013) 114.
- [24] R. Ohnishi, Y. Takahashi, A. Takagaki, J. Kubota, K. Domen, Niobium oxides as cathode electrocatalysts for platinum-free polymer electrolyte fuel cells, *Chem. Lett.* 37, (2008) 838.

- [25] L. Zhang, L. Wang, C. M. B. Holt, T. Navessin, K. Malek, M. H. Eikerling, D. Mitlin, Oxygen Reduction Reaction Activity and Electrochemical Stability of Thin-Film Bilayer Systems of Platinum on Niobium Oxide, *J. Phys. Chem. C* 114, (2010) 16463.
- [26] L. Zhang, L. Wang, C. M. B. Holt, B. Zahiri, Z. Li, K. Malek, T. Navessin, M. H. Eikerling, D. Mitlin, Highly corrosion resistant platinumniobium oxidecarbon nanotube electrodes for the oxygen reduction in PEMfuel cells, *Energy Environ. Sci.* 5, (2012) 6156.
- [27] D. Kowalski, Y. Aoki, H. Habazaki. Characterization of amorphous anodic Nb₂O₅ nanofilm for gas sensing, *ECS Trans.* 16, (2009) 57-65.
- [28] K. Naito, N. Kamegashira, N. Sasaki, Phase equilibrium in the system between NbO₂ and Nb₂O₅ at high temperatures, *J. of S.S. Chem.* 35, (1980) 305-311.
- [29] J. M. Gallego, C. B. Thomas, Preparation and characterization of thin films of NbO₂, *Thin Solid Films*, 98 (1982) 11-22.
- [30] F.J. Wong, N. Hong, S. Ramanathan, Orbital splitting and optical conductivity of the insulating state of NbO₂. *Phy. Rev. B* 90, (2014) 115135.
- [31] Inorganic Crystal Structure Database (ICSD) using POWD-12 + + (2004).
- [32] A. Magneli, G. Andersson, G. Sundkvist, Note on the crystal structure of niobium dioxide, *Acta Chem. Scand.* 9, (1955) 1402.
- [33] A.V. Arakcheeva, V.V. Grinevich, V.F. Shamrai, M. Meyer, G. Chapuis, KNb₄O₅F and NbO₂ crystal structures. Structural aspect of chemical decomposition of K_{2-x}Nb₄O₃(O,F)(3)F in the melt of sodium and potassium chlorides *Crystallogr. Rep.* 44, (1999) 2-7.
- [34] R. Pynn, J. D. Axe, R. Thomas, Structural distortions in the low-temperature phase of NbO₂, *Phys. Rev. B* 13, (1976) 2965.
- [35] T.S. Ercit, Refinement of the structure of zeta-Nb₂O₅ and its relationship to the rutile and thoreaulite structures, *Mineralogy and Petrology* 43, (1991) 217.
- [36] H. McMurdie, M. Morris, E. Evans, B. Paretzkin, W. Wong-Ng, Y. Zhang, Methods of producing standard x-ray diffraction powder patterns, *Powder Diffr.* 1, (1986) 342.
- [37] J. Waring, R. Roth, , H. J. Parker, Temperature-pressure phase relationships in niobium pentoxide, *Res. Natl. Bur. Stand.* 77A, (1973) 705.
- [38] B. Gatehouse, A. Wadsley, The crystal structure of the high temperature form of niobium pentoxide, *Acta Crystallogr.* 17, (1964) 1545.

- [39] M. Hanfland, U. Schwarz, K. Syassen, K. Takemura, Crystal structure of the high-pressure phase silicon VI. Phys. Rev. Lett. 82, (1999) 1197.
- [40] D. Music, Y. Chen, P. Bliem, R. W. Geyer, Amorphous-crystalline transition in thermoelectric NbO₂, J. Phys. D: Appl. Phys. 48 (2015) 275301.